

Center for X-Ray Optics

1992

Materials Science Division
Lawrence Berkeley Laboratory
University of California
Berkeley, California 94720

LBL-34462

Printed August 1993

This work was supported by the Director, Office of Energy Research, Office of Basic Energy Sciences, Materials Science Division, of the U.S. Department of Energy under Contract No. DE-AC03-76SF00098, by the U.S. Department of Defense, Air Force Office of Scientific Research under Contract No. F49620-87-K-0001, and by the Advanced Research Projects Agency under ARPA Order AO-8335.

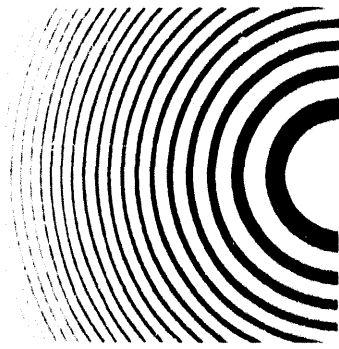
MASTER

DISTRIBUTION OF THIS DOCUMENT IS UNLIMITED



Contents

Center for X-Ray Optics	1
Staff Listing	1
Soft X-Ray Imaging with Zone Plate Lenses	2
Development of Fresnel Zone Plate Lenses	2
Soft X-Ray Microinterferometer for Materials Studies	3
Biological X-Ray Microscopy	5
Extreme Ultraviolet Lithography for Nanoelectronic Pattern Transfer	7
A Next Generation Nanowriter	8
Reflective Masks for Extreme Ultraviolet Lithography	9
Multilayer Reflective Optics	11
Studies of Roughness and Diffuse Scattering from Mirrors	11
Controlling Multilayer Period Variation for Imaging Applications	13
Tarnishing and Restoration of Mo/Si Multilayer X-Ray Mirrors	14
Electron Beam Microanalysis of Light Elements	15
EUV/Soft X-ray Reflectometer	15
Photoemission Microscopy with Reflective Optics	17
Spectroscopy with Soft X-Rays	18
Monochromators and Spectrometers	19
Spatially and Temporally Coherent Beamlines	19
High Resolution VUV Monochromator for the Chemical Dynamics Beamline ..	20
High Resolution Monochromator for Carbon Related Studies	21
Hard X-Ray Microprobe	21
X-Ray Microprobe Beamline at the ALS	22
Coronary Angiography	23
Atomic Scattering Factors	24
Publications and Presentations	26



CENTER FOR X-RAY OPTICS

In 1992 the Center for X-Ray Optics (CXRO) continued its two complementary roles: demonstrating the capabilities and usefulness of the x-ray and ultraviolet regions of the spectrum and developing equipment and techniques to make those capabilities widely and readily available. Efforts continue to develop state of the art x-ray lenses and mirrors, monochromators optimized for high resolution and throughput, optical systems for the utilization of partially coherent radiation, and applications across the physical and life sciences.

High-resolution x-ray microscopy continues to be a prominent activity. Soft-x-ray microscopy based on Fresnel zone-plate lenses has provided images of features as small as 300 Å in experiments at the Berlin Electron Synchrotron (BESSY). Spatially resolved studies of materials have been conducted with colleagues at both Wisconsin and Brookhaven. Biomicroscopy studies have been explored with colleagues at Göttingen and Stony Brook. In the hard-x-ray regime, a microprobe, based on multi-layer-coated reflective optics, has achieved 2-μm spatial resolution at the National Synchrotron Light Source (NSLS) and has been used in a large number of applications in the life and physical sciences. The microprobe is presently in use at ESRF in Grenoble, and will soon be used among the first experiments at LBL's newly commissioned Advanced Light Source (ALS).

Scientific and Technical Staff

D. Attwood (*director*)
I. Underwood (*deputy director*)
K. Jackson (*associate director*)
E. Anderson
P. Batson
V. Boegli
I. Bokor
K. Chapman
R. Delano
P. Denham
I. Gullikson
I. K. Gustafson
B. Henke (*emeritus*)
M. Hur
D. Kemp
S. Klingler
M. Kotke
J. Kortright
W. Low
H. Medeck
W. Meyer Ilse
I. Muray
I. Swan
R. Tackaberry
A. Thompson

Administrative Support

P. Butler
E. Fessman
M. Holloway
B. Robbins

Affiliate Members

N. Coglio, ILL
E. Cerrina, University of Wisconsin
I.H.P. Chang, IBM-Yorktown Heights
C. Ditmore, ILL
D. Kern, IBM-Yorktown Heights
I. Kirz, SUNY-Stony Brook
D. Matthews, ILL
E. Namtaka, Tohoku University and U. of Maryland
M. Richardson, University of Central Florida
G. Schmahl, University of Göttingen
G. Sommariva, ILL
D. Sweeney, ILL
Y. Vladimirov, Louisiana State University

Students

H.R. Begunistan
S. Bhagi
I. Chiu
I. Fu
K. Goldberg
K. Gomez
A. Irtel von Brendort (Göttingen)
N. Iskander
O. Jacob
X. Lu
D. Lee
B. Lum
J. Maser (Göttingen)
K. Nguyen
I. Nguyen
M. Nusshardt (Dortmund)
S. Oh
A. Padmaperuma
R. Pineda (Intel)
F. Tam
M. Varghese
C. Wallon
K. Watson
M. Wei
A. Yu
A. Zege

In the long-term effort to develop high-reflectivity multilayer coatings for extreme-ultraviolet and soft-x-ray optical elements, such as mirrors and gratings, we continued investigating the structure and stability of various multilayer pairs and developed a new, highly versatile reflectometer based on a laser-plasma x-ray source and a high-throughput monochromator.

A new program in projection lithography has been initiated whose goal is to provide critical metrologies and optical test capabilities for a national program in nanoelectronic pattern transfer. This joint initiative brings researchers from CXRO and the University of California at Berkeley together with representatives of the semiconductor industry. The goal is to further the use of extreme ultraviolet (EUV) radiation in the fabrication of computer chips with feature sizes of order $0.1 \mu\text{m}$. The photon beams from the ALS are well suited to this research, as is our experience with high resolution electron beams and nanometer-scaled metrologies for fine pattern writing.

With completion of the ALS anticipated in 1993, a number of beamline and endstation projects are underway there, including a high resolution zone plate microscope, "at wavelength" (130 \AA) interferometry of reflective optics for nanoelectronic pattern transfer, a metrology beamline for spatially and spectrally resolved absolute spectrometry, and a hard x-ray microprobe as mentioned above. A new high resolution electron beam "nanowriter" for diffractive optics, mask writing and materials research is also under development.

Extending high-resolution visible-light and ultraviolet imaging techniques into the soft-x-ray region of the spectrum offers several special advantages. The relatively short wavelengths, ranging from several angstroms to perhaps 100 angstroms, permit researchers to both "see" and "write" smaller patterns. Furthermore, the associated photon energies, ranging from approximately 100 to several thousand electron volts (eV), span the primary resonances of many elements. Resonances constitute a sensitive mechanism for element identification, for elemental mapping, and, in some cases, for determination of chemical bonding. Working with collaborators worldwide we helped to advance the technology of soft-x-ray imaging and continued to demonstrate potential applications in both the physical and life sciences. Features as small as 300 \AA may be seen in our best images.

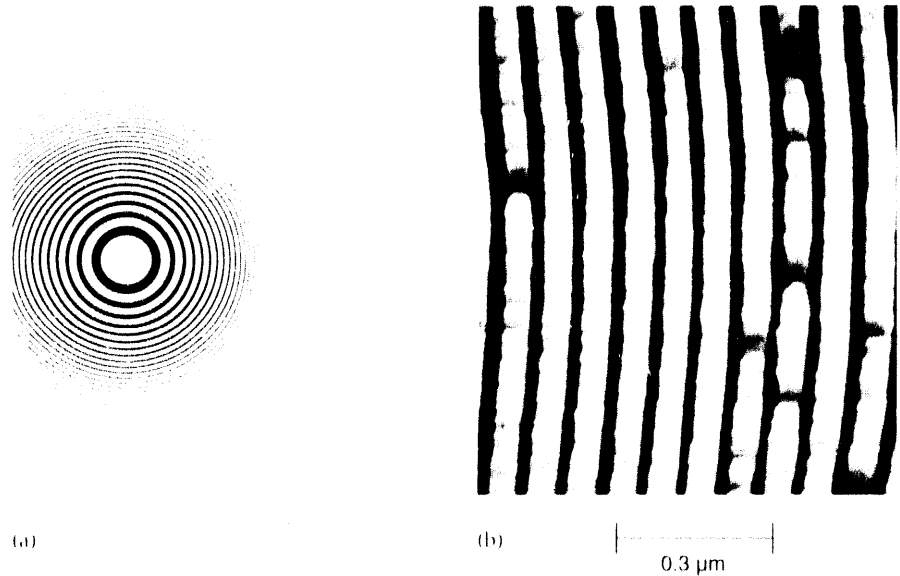
In microscopy with soft x-rays, the key optical component that ultimately determines performance is the objective lens. Ordinary refractive lenses like those used for visible light, which transform the phase of a wavefront without changing the amplitude, cannot be used at x-ray wavelengths because available materials do not give enough phase shift and are not sufficiently transparent. To date the best resolution obtained in this spectral region has been obtained with Fresnel zone plate lenses. Zone plates are thus the lenses of choice for the highest spatial resolution, particularly for energies greater than 200 eV.

In pressing toward the fundamental diffraction limit of lens performance, accurate placement of the zones (alternate bands of transmissive and opaque material) is important. The maximum placement error should be less than a fraction of the smallest zone width of the lens. This is a

Soft-X-Ray Imaging with Zone-Plate Lenses

Development of Fresnel Zone-Plate Lenses

Figure 1. This Fresnel zone-plate lens, made of nickel, is representative of our state-of-the-art accomplishments. It has a smallest zone width of 350 Å. (a) shows the central zones and (b) shows the fine structure of some of the smaller zones.



XBB 937 5004

XBB 937 5005

formidable challenge, since our highest-resolution lenses, like the one shown in Figure 1, have zone widths of order 350 Å. Achievement of the required accuracy at these dimensions, especially across large (50- μ m-diameter) lenses, is at the frontier of metrology and microfabrication.

In collaboration with researchers from the University of Göttingen, we have been using and characterizing the high resolution zone plates in the Göttingen x-ray microscope at the Berlin Electron Synchrotron (BESSY). Although measurements of the microscope's optical performance indicate that the diffraction limit has not been reached, images of test patterns show that features as small as 300 Å are visible. Our newest nickel zone plate lenses have achieved both high spatial resolution and high diffractive efficiency.

Soft X-Ray Microinterferometer for Materials Studies

The accurate measurement of the x-ray optical properties of materials, both attenuation and phase shift, is technologically and scientifically important. A new type of interferometer has been designed and build to make direct measurements of the phase shift as well as attenuation through a test sample on a sub-0.1 μ m spatial scale. This interferometer uses all diffractive optics: two gratings and a zone plate, in a configuration similar to an imaging x-ray microscope. Figure 2 shows the physical set up. A grating with a period of $\Lambda = 0.4 \mu$ m is imaged by a zone plane lens ($D = 100 \mu$ m, $\Delta r = 0.06 \mu$ m). In the zone plate back focal plane the diffracted order of the grating form a series of spots for the 0th, +/-1, +/-2,... diffracted orders. An aperture blocks all orders except the +1 and -1. At the image plane these two orders recombine to form an image of the original grating, which has half the magnified period since the zero order is missing. Because the period of this interference pattern is smaller than the resolution of the micro-channel plate detector (MCP), a final grating is used to form a Moiré pattern that is observable on the MCP. Figure 3 shows the sub-micron resolution flexure stages used to position the zone plate, aperture, and sample each in X, Y, and Z. If the sample under test is

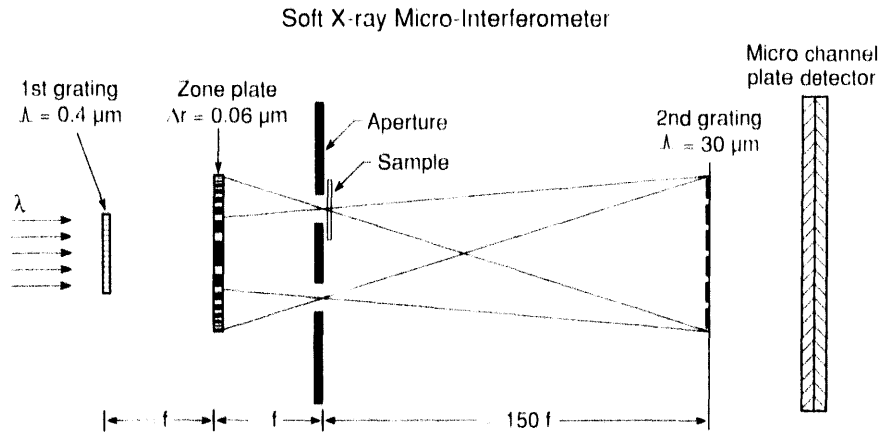


Figure 2. Schematic layout of the soft x-ray microinterferometer.

XBI 937-4822

inserted in only one of the diffracted orders (which are $30 \mu\text{m}$ apart), the amplitude (i.e., contrast) and relative phase of the observed Moiré fringes spread out over the entire MCP area. A sine pattern is measured by translating the final grating through one or more periods while recording the x-ray count rate as a function of position. Preliminary experimental results at the NSLS X1 beamline demonstrate that the interferometer works and that fringe patterns have been obtained. Further effort is needed to accurately measure the optical constants of materials on a sub- $0.1 \mu\text{m}$ scale.

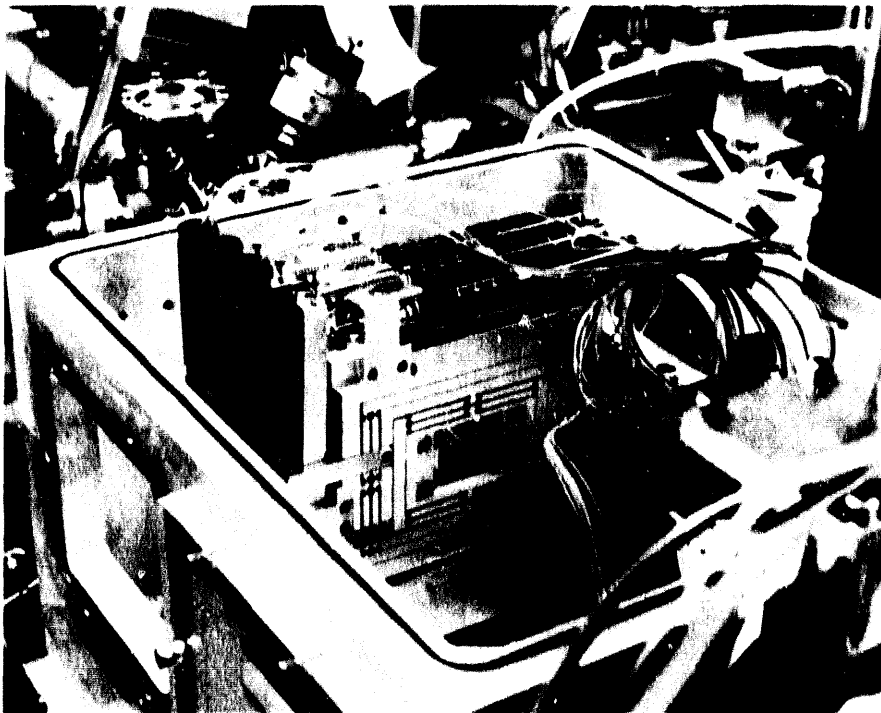


Figure 3. Soft x-ray microinterferometer housing with zone plate, aperture, and sample stages.

CBB 937-4854

Biological X-Ray Microscopy

Compared to visible light microscopy, x-ray microscopy has a greatly improved resolution. The key optical elements in achieving this resolution are the zone-plate lenses described above. Although x-ray microscopy does not compete with electron microscopy in terms of resolution, it offers unique advantages, including the ability to image thick (1-10 μm) intact samples, and to do this in an aqueous physiologically relevant environment. The method is based on the interaction of x-rays with matter in the wavelength range from 22-44 \AA (the so-called "water window"). In this range, water absorbs relatively weakly, allowing contrast to be provided by naturally occurring cell components such as proteins, nucleic acids, and carbohydrates. Because of the penetrating power of x-rays, information can be obtained from thick samples that are not accessible to other techniques, including high voltage electron, atomic force, and near-field microscopies. The x-ray microscope can also be used as a high resolution analytical tool. In conjunction with a tunable synchrotron-based x-ray source, the specific absorption properties of different elements can be used to obtain elemental maps and other chemical information from the samples.

X-ray microscopes can be either conventionally designed imaging x-ray microscopes or scanning x-ray microscopes. The most elaborate microscopes of either type are the Göttingen imaging x-ray microscope at BESSY in Berlin and the scanning x-ray microscope at the NSLS, Brookhaven National Laboratory. The two microscopes serve complementary needs. Using an uncomplicated design, the imaging microscope provides images with the highest resolution combined with the shortest exposure times. The scanning microscope offers a distinct advantage of high spatial resolution images with minimal radiation dose. We have conducted experiments at both facilities during the past year and conducted a design effort to build both microscope types at the Advanced Light Source.

The high resolution of x-ray microscopy is achieved with zone plate lenses, which we build with an over all efficiency of 7.3% and an outermost zone width of 350 \AA —closer to the theoretical limit than any other zone plate with this resolution. These zone plates are regularly used with the scanning electron microscope at Brookhaven, and the highest resolution experiments to date have been performed with these zone plates on the imaging x-ray microscope at BESSY. The high efficiency of these zone plates enables reduction of the radiation dose to a biological sample, while a further reduction is achieved by using a highly efficient detector. To utilize these advantages, we installed a special electronic camera on the BESSY microscope using a back-illuminated thinned CCD as a recording device, which achieves a 62% efficiency at the most used x-ray wavelength of 24 \AA . This camera reduces both the exposure time and the radiation applied to the sample, each by more than an order of magnitude.

Our experiments at the existing x-ray microscopes have addressed two needs: first was evaluation of the performance of such critical parts of x-ray microscopes as zone plates and detectors. Second was enhancement of our knowledge of preparation techniques, contrast mechanisms, and related topics. Examples of biological samples imaged using the instruments at BESSY and Brookhaven National Laboratory are shown in Figures 4 and 5.

The Center for X-Ray Optics has begun to design complementary imaging and scanning x-ray microscopes for the Advanced Light Source to form a Biological X-Ray Microscopy Resource Center. Because the ALS is the brightest source of tunable x-rays available worldwide, these microscopes will combine the highest possible resolution with shortest possible exposure times. The first microscope at the ALS will be an imaging type using bending magnet radiation, to be available in 1994.

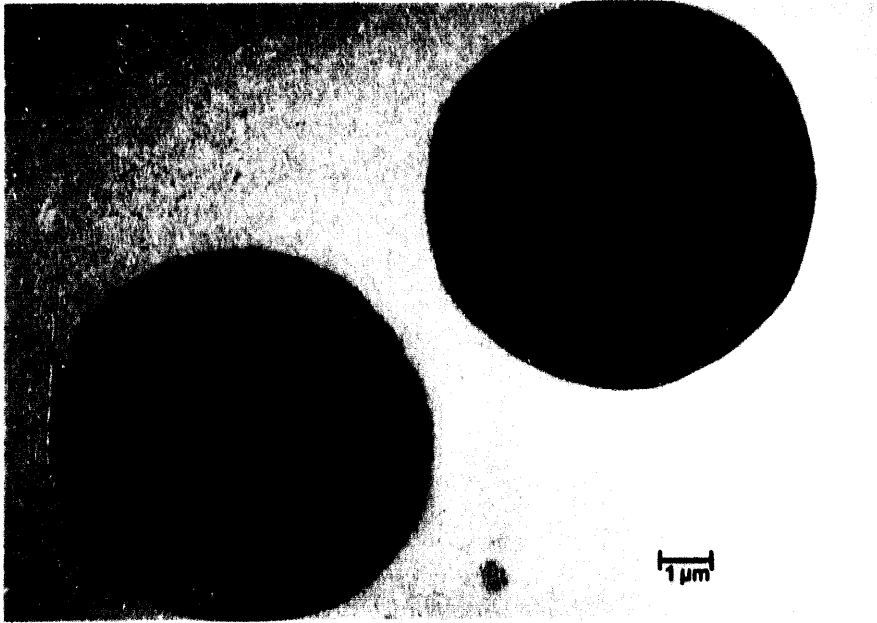


Figure 4. Intact human red blood cells, one infected by malaria parasites, both imaged with soft x-rays. These studies indicate that x-ray microscopes are well suited to studying the development of the parasite within the cell, and may provide useful information regarding the pathology of the disease. These images are part of a study by Drs. C. Magowan and M. Moronne (LBL). The image was taken with the Göttingen x-ray microscope at BESSY in Berlin.

BBC 937 4855

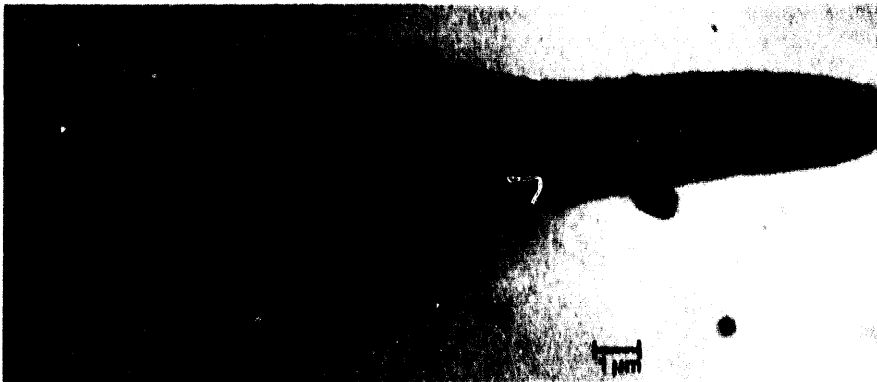


Figure 5. Spermhead of a marsupial mouse (*Sminthopsis*) taken with the Göttingen x-ray microscope at BESSY using the new back-illuminated CCD camera and a high efficiency nickel zone plate (350 Å outermost zone width). This image is part of a study by Drs. William Breed (U. of Adelaide) and Rodney Balhorn (LLNL).

XBB 937 5002

Extreme Ultraviolet Lithography for Nanoelectronic Pattern Transfer

Since the creation of the first integrated circuit in 1960 there has been an ever increasing density of devices manufactured on semiconductor substrates. The very large scale integration (VLSI) era from the mid 1970s to the present has seen chip densities from 100,000 transistors per chip to over 1 million per chip. This increasing device count was accomplished by a shrinking minimum feature size that includes linewidth, spacing, and contact dimensions, from 2 μm in the late 1970s to less than 0.75 μm in current 4-megabit dynamic random access memories (DRAMs). The challenge to continued U.S. industrial competitiveness in microelectronics will be development of new techniques of lithography and pattern transfer at minimum feature sizes of 0.1 μm and smaller. The lithography program at the Center for X-Ray Optics focuses on the enabling technologies that are essential for EUV optical imaging systems; imaging systems that will be required for 0.1- μm features and 1-gigabit integrated circuits by the year 2000. The program concentrates on the development of EUV interferometry for testing optics at a wavelength of 130 \AA , nanofabrication facilities for diffractive optics and reflective masks, high placement accuracy over large areas, and related research activities in optics, device physics, pattern transfer, and requisite metrologies.

New facilities will include bending magnet and undulator beamlines at the Advanced Light Source. The undulator beamline will have a unique EUV interferometer for "at wavelength" characterization of high numerical aperture reflective optics based on the use of partially coherent undulator radiation. A bending magnet beamline at the ALS will be fitted with both EUV and soft x-ray metrology stations for spatially and spectrally resolved absolute spectrometry, including precise measurements of mirror reflectivity, resist sensitivity, optical efficiency, refractive index, and other quantities.

In addition, a nanofabrication facility, described below, with next generation direct-write electron-beam capability (a "nanowriter") for making best-in-the-world diffractive x-ray optics, reflective mask patterns, and other structures is being built.

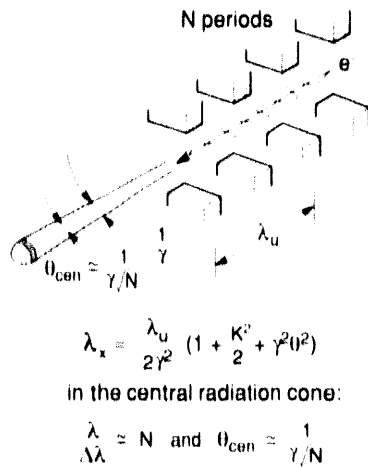
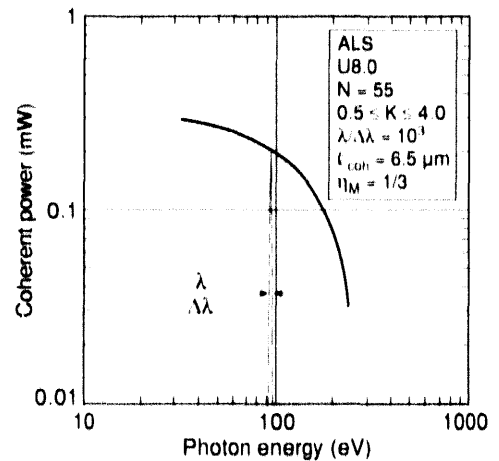


Figure 6. Spatially and temporally filtered radiation at the ALS will be used for "at-wavelength" interferometric testing of optics. The beamline design is shown in Figure 19.



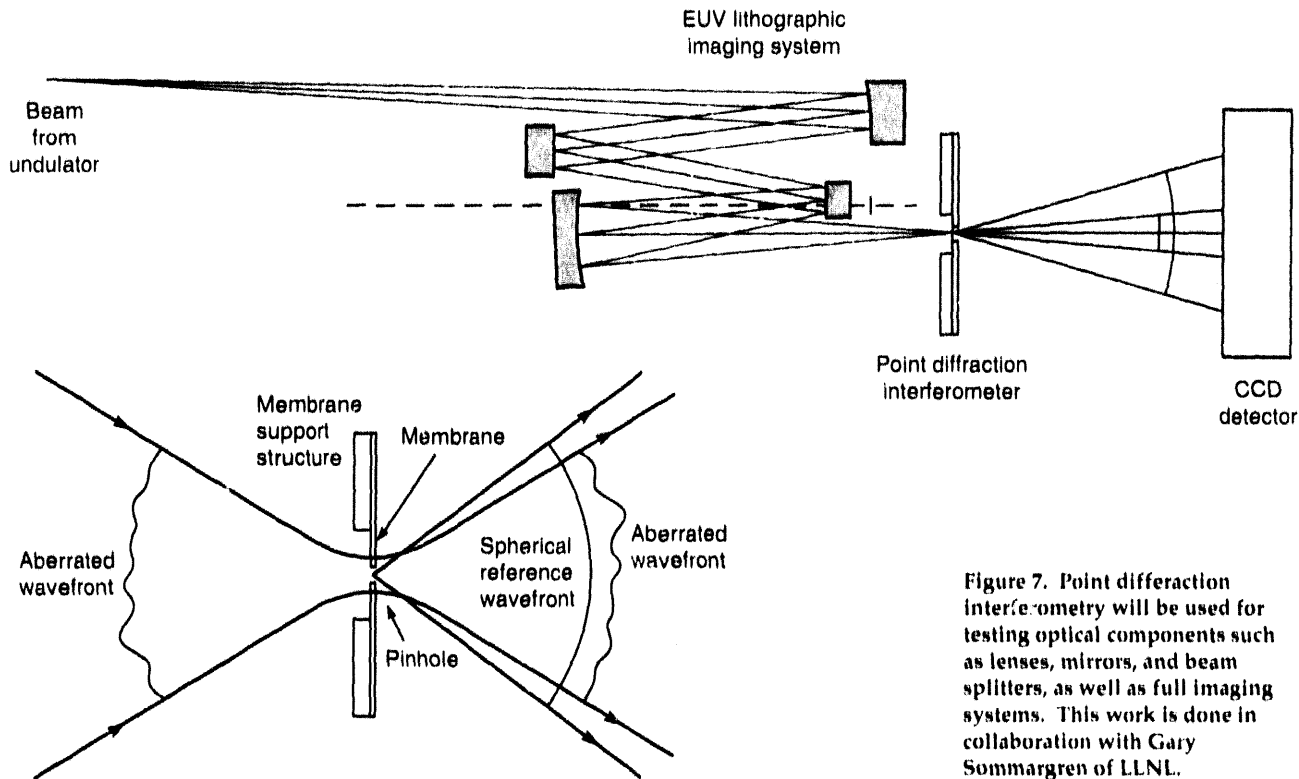


Figure 7. Point diffraction interferometry will be used for testing optical components such as lenses, mirrors, and beam splitters, as well as full imaging systems. This work is done in collaboration with Gary Sommargren of LLNL.

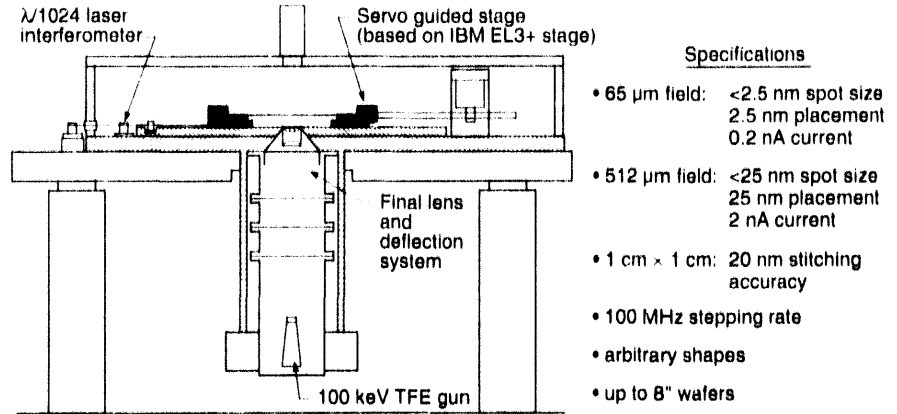
XBL 937-4824

For fabrication of state of the art diffractive optics (zone plates and gratings), electron-beam nanolithography is a key technology. To overcome limitations with commercially available electron-beam machines, LBL has taken on an ambitious project to develop a next-generation "nanowriter." The nanowriter and other instrumentation will allow research in the areas of high resolution diffractive optics, nanoelectronic patterning, materials processing, studies of quantum transport device physics, and the development of requisite metrologies for the overlay of 0.1- μm patterns across square centimeter areas in future nanoelectronic devices. Our goal is to build a working machine that is superior to existing systems in terms of resolution, placement accuracy, and throughput. Some of the aggressive specifications to be met are a 2.5-nm spot size within a 100- μm diameter field size, less than 25-nm stitching error between fields over square centimeter dimensions, and up to 100-MHz beam stepping rate with arbitrary shape exposure.

During the development, great emphasis is given to keeping the system flexible, expandable, and tunable to meet different requirements for placement accuracy, minimum feature size, and moderate throughput. Of the 14 subsystems identified for the nanowriter, three represent a special challenge in that their specifications reach beyond what has been done to date. Two of them, the integrated final lens and deflection system, and the ultra-high precision specimen stage, will be co-developed by CXRO

A Next-Generation Nanowriter

Figure 8. Schematic of the "nanowriter" electron-beam system under development by LBL and industrial partners.



XBL 9212-5863

scientists and an outside vendor. The third, the high-speed digital pattern generator, is currently under development by CXRO.

Other subsystems, including job preparation software and proximity effect correction, as well as the overall tool control hardware and software, are also being developed within CXRO, which will also be responsible for overall project management and system integration. Negotiations have been started with IBM Research, where prototypes of the tool control system and portions of the proximity correction are being used to control several nanolithography electron-beam machines. The nanowriter is expected to be operational in 1996.

Reflective Masks for Extreme Ultraviolet Lithography

The development of reflective masks is a critical component of the emerging program in extreme ultraviolet lithography. A reflective mask is made by patterning an absorber layer above a multilayer reflective coating. To be imaged with fidelity onto the wafer, all factors that affect its imaging characteristic must be well understood. The abrupt topography of the absorber layer and the distributed reflection from the coating make calculations of the reflected image complex. As a result, electromagnetic simulations using time-domain finite-difference techniques are used to study the effects of topography and multilayer coating defects on the reflected areal image.

In early investigations we find that the illumination angle should be of no more than 10 degrees off-normal incidence and that only a thin absorber layer, approximately 100 nm, of germanium or carbon is needed for good image contrast. With near normal-incidence illumination and a thin absorber layer, the absorber overlayer reflective mask is relatively insensitive to variations in incidence angle in absorber profile, making it a robust mask geometry.

The effect of multilayer defects on the reflected image, however, can be dramatic. For instance, a substrate defect of one tenth the resolution limit can produce a 70% reduction in image intensity. Experimental studies are underway to confirm these predictions. In addition to pattern transfer studies, high resolution transmission electron microscopy and scanning tunneling microscopy are being used to study the propagation of a substrate defect through the multilayer stack and its effect on the multilayer structure.

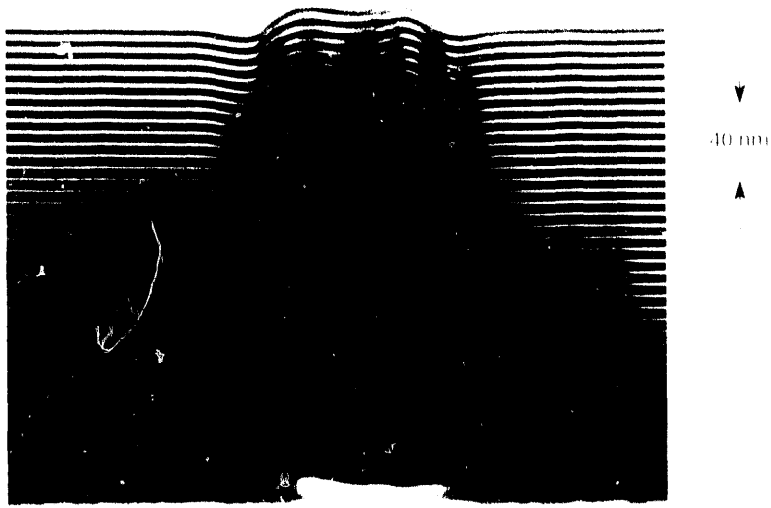


Figure 9. Defect propagation through a multilayer stack as seen with high resolution electron microscopy.

010-10-0007

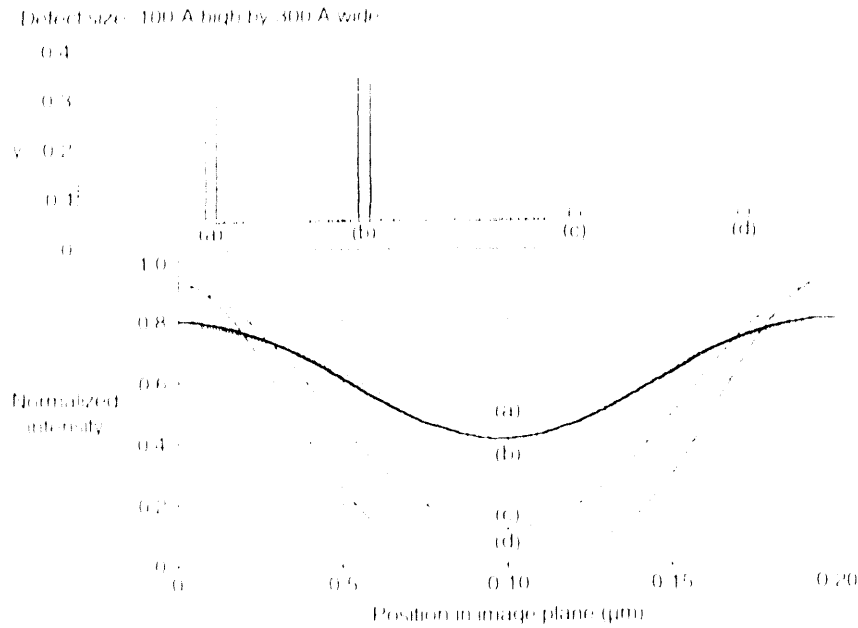


Figure 10. Various models for defect propagation through a multilayer mask (top), and simulations (bottom) of the effect on areal image intensity.

010-10-0007

Multilayer Reflective Optics

Multilayer coatings are effective reflectors of x-rays over a broad wavelength range. The wavelengths and angles of incidence for which they are highly reflective are determined by the Bragg Equation with the d spacing equal to the period of the multilayer; that is, the sum of the thicknesses of one high-Z and one low-Z layer. Our effort encompasses fabricating multilayers via sputtering techniques, advancing the applications of multilayers in a variety of forefront experiments, and conducting fundamental research into multilayers themselves to improve them and elucidate their performance limits.

In the U.S and abroad, multilayers fabricated in our laboratory have been incorporated into a wide variety of x-ray optical systems at photon energies ranging from the extreme ultraviolet (EUV) to the hard x-ray regions of the spectrum. In the EUV and soft x-ray regions multilayer applications include simple dispersing elements for spectroscopy, normal incidence imaging optics of interest, e.g., in projection lithography, polarization controlling and converting devices, and coatings on gratings to extend their high energy range. In the hard x-ray region applications typically take advantage of the broad bandwidth of multilayers compared to natural crystals, and include broadband dispersing elements, power filtering mirrors, and coatings for microfocusing mirrors.

Studies of Roughness and Diffuse Scattering from Mirrors

Interface roughness reduces specular reflectance and produces diffuse scattering, both of which are critically important in specifying the performance of x-ray mirrors. These effects are especially severe for multilayer mirrors because they operate at large scattering vector or momentum transfer compared to total reflection mirrors, where they are most pronounced. We study the roughness of x-ray mirrors by measuring the specular reflectance and diffuse scattering from a variety of samples, including flat polished substrates, sputtered single films, and multilayers. The surfaces are also measured by optical interferometry and atomic force microscopy to compare the roughness values obtained from these different techniques. Microstructural characterization using TEM and high-angle x-ray scattering are applied to multilayers and films in some cases. In addition to providing fundamental data on x-ray mirror performance, these measurements allow us to test theoretical predictions of how interface roughness affects mirror performance. We are especially interested in studying how roughness evolves with polishing (in the case of mirror substrates) and with deposition (in the case of single or multilayer film deposition), and how thin film microstructure affects roughness.

One study, illustrated in Figure 11, investigates how substrate roughness evolves with polishing, and how the different levels of polishing affect the performance of multilayer mirrors deposited on those substrates. The substrates were fused-silica optical flats polished to four different levels of microroughness ranging from 0.2 to 11 Å as determined by the polisher using visible interferometry. These roughness values span the range typical of most well polished x-ray mirrors, with the smoothest samples comparable to the best superpolished mirrors available. The x-ray reflectance and scattering measurements were made at the Stanford Synchrotron Radiation Laboratory using 1.38-Å radiation. Figures 11 (a) and (b) show the specular reflectance from the substrates alone and from an identical W/C multilayer with $d = 30.6$ Å deposited onto those substrates. Figure 11(c) shows diffuse scattering from the bare substrates

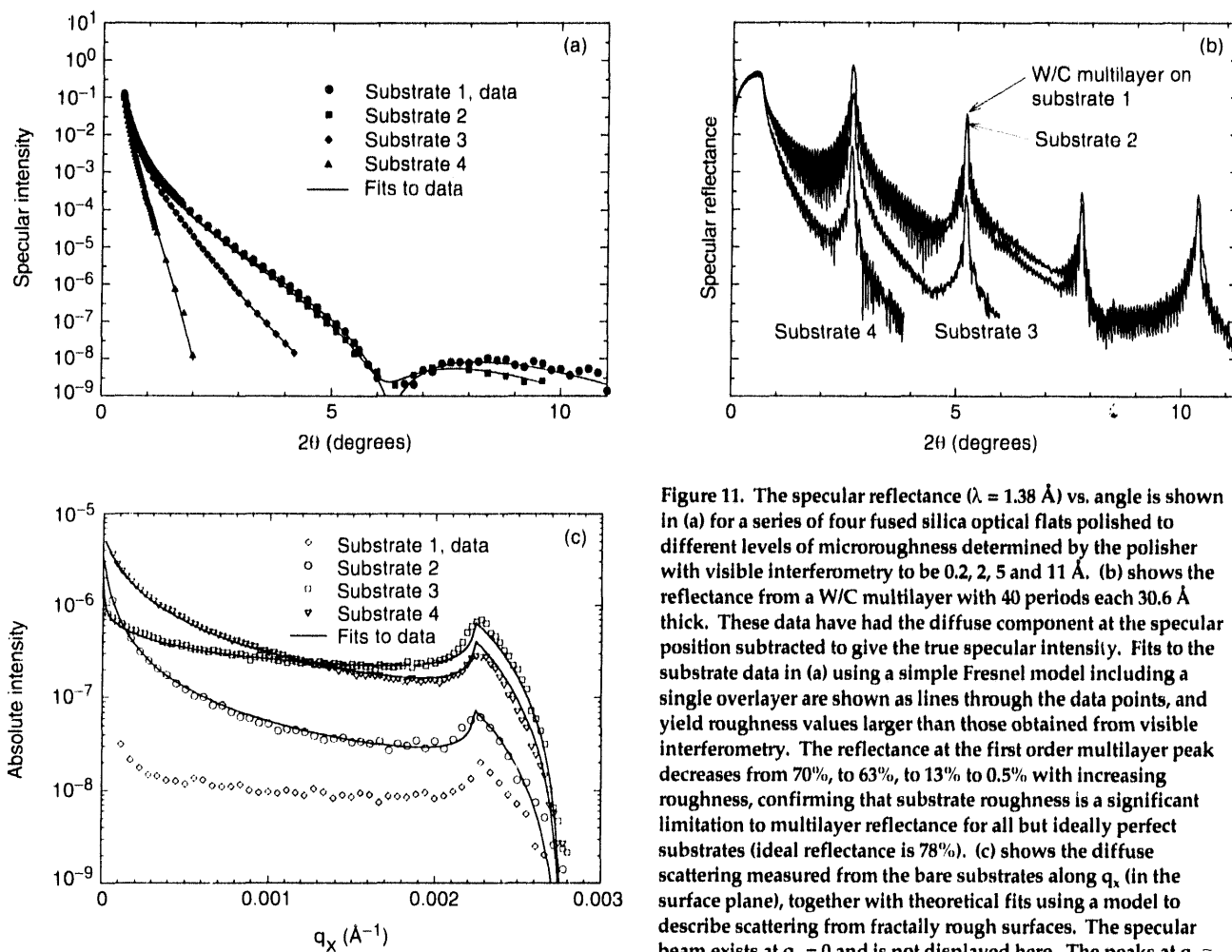


Figure 11. The specular reflectance ($\lambda = 1.38 \text{ \AA}$) vs. angle is shown in (a) for a series of four fused silica optical flats polished to different levels of microroughness determined by the polisher with visible interferometry to be 0.2, 2, 5 and 11 \AA . (b) shows the reflectance from a W/C multilayer with 40 periods each 30.6 \AA thick. These data have had the diffuse component at the specular position subtracted to give the true specular intensity. Fits to the substrate data in (a) using a simple Fresnel model including a single overlayer are shown as lines through the data points, and yield roughness values larger than those obtained from visible interferometry. The reflectance at the first order multilayer peak decreases from 70%, to 63%, to 13% to 0.5% with increasing roughness, confirming that substrate roughness is a significant limitation to multilayer reflectance for all but ideally perfect substrates (ideal reflectance is 78%). (c) shows the diffuse scattering measured from the bare substrates along q_x (in the surface plane), together with theoretical fits using a model to describe scattering from fractally rough surfaces. The specular beam exists at $q_x = 0$ and is not displayed here. The peaks at $q_x \approx 0.0023 \text{ \AA}^{-1}$ occur when the incident or reflected angles equal the critical angle, and indicate that the measured scattering results from surface not bulk fluctuations. The fractal model can fit scattering from all but the smoothest surface, whose scattering looks like white noise over most of this frequency range. The entire data set is consistent with growth of smooth W and C layers which conform successively to the roughness of the substrate over the range of frequencies measured.

XBL 937-4827

measured with rocking scans, together with theoretical fits to these data using a model developed to describe scattering from fractally rough surfaces. Together the specular and diffuse scattering are extremely sensitive to the magnitude and nature of interface roughness.

This study demonstrates that, for high quality multilayers which form smooth and well-defined layers like the W/C multilayers studied here, multilayer reflectance is limited by substrate roughness. This limitation becomes increasingly severe as the multilayer period decreases, and can be the dominant factor limiting multilayers from achieving their theoretical ideal performance as wavelengths approach the C edge and the water window. This study also emphasizes the need for continued substrate development aimed at achieving ever smoother surfaces.

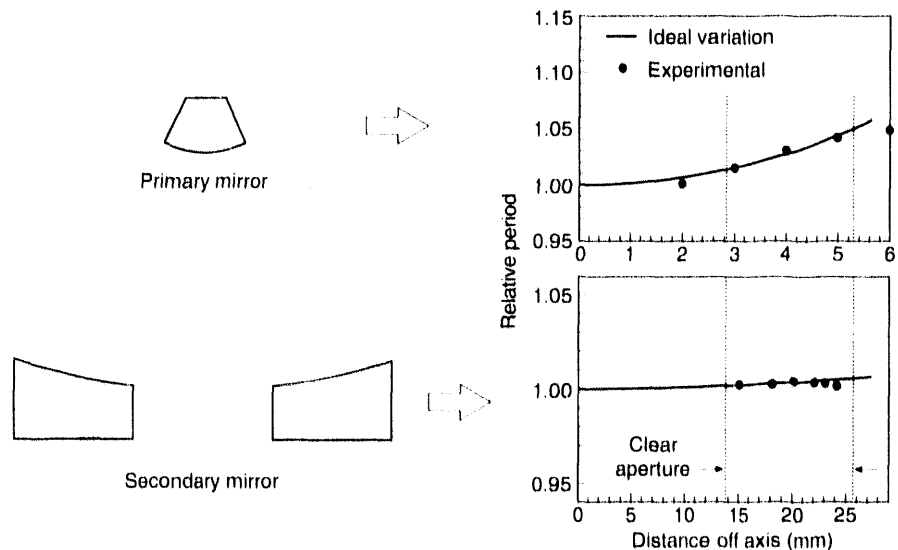
Controlling Multilayer Period Variation for Imaging Applications

Figure 12. The need to control multilayer period (d) variation on focusing optics arises because Bragg's law must be satisfied for each ray at each mirror at a fixed wavelength to have an achromatic imaging system. The primary and secondary mirrors of the 20 \times demagnifying Schwarzschild objective at the left present a range of angles that prescribe the ideal d variations at the right. The tolerance needed to match this prescribed variation of several percent is set by the multilayer bandpass, which decreases with wavelength to one percent or less at 68 Å where Ru/B₄C multilayers have useful reflectance. We have developed techniques to specifically tailor the d variation on the curved surface of each mirror by introducing masks between the source and substrate to systematically reduce deposition much like dodging in the printing of a photograph. Equally important is the ability to measure and verify these d variations using spatially-resolved, near normal incidence reflectometry. The measured d variations are shown in the plots. The peak reflectance of the Ru/B₄C multilayers across each mirror is roughly 15% at 68 Å.

Multilayer-coated focusing systems for XUV imaging, by their very nature, generally require laterally graded multilayer period or thickness across the clear aperture of mirrors to optimize performance. This requirement stems from the variation of incidence angles given by the optical design, and the inherent finite bandwidth of x-ray multilayers. The ideal period (d) variation at each mirror is prescribed for small-field imaging systems by the variation in incidence angle (from grazing) across the clear aperture through the Bragg condition for constructive multilayer interference, $\lambda = 2d\sin\theta$. This is illustrated for a 20 \times demagnifying Schwarzschild objective in Figure 12, which shows the how the period should vary across each mirror to avoid unwanted intensity and phase variations across the clear aperture. The actual d variation should conform to this prescribed ideal variation to a tolerance of a fraction of the multilayer bandwidth.

The bandwidth of soft x-ray multilayers scales with wavelength, and hence so does the need to precisely control the multilayer period variation. Mo/Si multilayers for use at > 125 Å have bandwidths of 4-5 percent or larger, leading to relatively generous tolerances for the control of d . Ru/B₄C multilayers have high reflectance at > 66 Å and bandwidths of 1 percent or less, requiring the development of new techniques to control and verify the d variation on this and similar optics. These narrow bandwidths not only necessitate improved control of d variation across each individual curved surface, but also increase the demands on matching the coatings of different mirrors in a compound imaging system.

We have developed experimental techniques to control and verify the d variation of narrow bandwidth multilayers on a 20 \times demagnifying Schwarzschild. Two issues are key in these developments, the ability to precisely control d variation during deposition over steeply curved surfaces, and the ability to precisely measure the multilayer reflectance spectra with adequate spatial resolution on these curved surfaces. We obtain control over deposition profile by introducing masks between the source and substrate to alter the deposition profile in a specifically desired manner. Spatially resolved measurement of d variation across these



XBL 927-5755

curved surfaces is accomplished with at-wavelength, near normal-incidence reflectance measurements using our newly developed laser-plasma based reflectometer. An iterative approach of deposition profile modification and spatially resolved reflectometry converges on an acceptable solution to the coating problem, and demonstrates unprecedented control of multilayer coatings on curved surfaces. These techniques are generally applicable to condenser and imaging optics of interest for soft x-ray projection lithography, as well as other multilayer-coated focusing systems.

Multilayer x-ray mirrors of molybdenum and silicon operating at normal incidence at wavelengths just longward of the Si L_{II,III} absorption edges are a key component in the development of extreme ultraviolet projection lithography. Because the achievement and maintenance of high reflectivity surfaces are vital, it is important to know if Mo/Si multilayers change reflectivity with time, and a series of experiments was carried out to investigate this possibility. Mo/Si multilayer mirrors were prepared to reflect 148 Å radiation at normal incidence with 50 layer pairs, and $d = 76.2$ Å. The reflectors were prepared both with molybdenum as the terminating layer (Mo on top) and with Si as the terminating layer (Si on top). The reflectivity of these multilayers on silicon wafers was measured immediately after deposition using the laser plasma reflectometer and then at intervals of a few days. Between measurements the samples were stored in laboratory air. The results are shown in figure 13. Immediately after deposition both sets of mirror samples had a reflectivity of between 61 and 63%, but over a period of months the reflectivity of the Mo-on-top samples decayed exponentially to an asymptotic value of about 48%, while the Si-on-top mirrors maintained their original reflectivity. Chemical analysis of the surface of the aged Mo-on-top mirrors showed that the topmost molybdenum layer had become oxidized to MoO₃ and MoO₂, and computational modeling showed that such oxidation could explain the drop in reflectivity. Since the observed decrease in reflectivity for the Mo-on-top mirror would lead to a decrease in throughput by a factor of 4 for a seven-element projection lithography system, it is clearly preferable to fabricate the mirrors with silicon as the topmost surface.

Tarnishing and Restoration of Mo/Si Multilayer X-Ray Mirrors

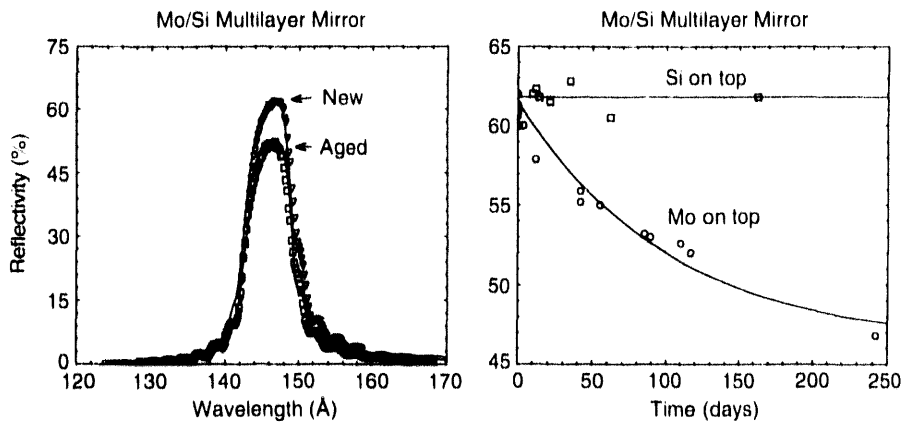


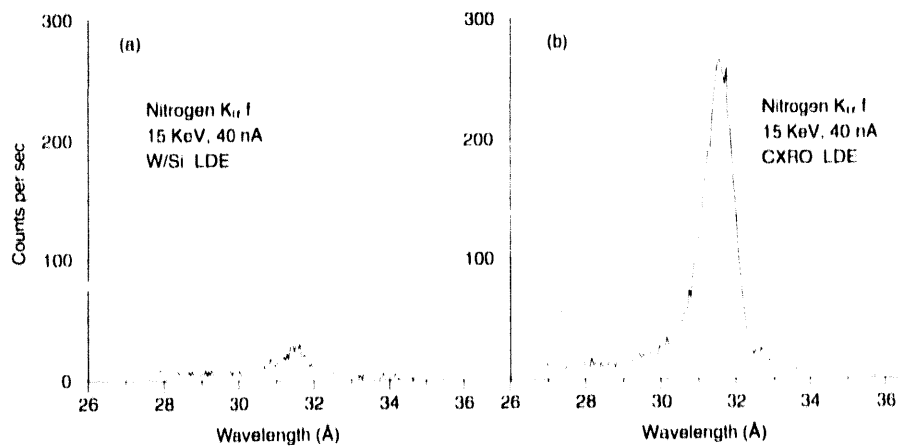
Figure 13. *Left:* Reflectivity as a function of wavelength for a Mo/Si multilayer mirror designed to reflect 148 Å at normal incidence. This mirror had Mo as the top layer; the two curves show the reflectivity just after deposition (triangles) and after storage in air for 244 days (squares). *Right:* peak reflectivity vs. time for the same multilayer compared with the peak reflectivity vs. time for an identical multilayer having silicon as the top layer. The silicon protects the molybdenum against oxidation, which is the cause of its degraded reflectivity.

XBL 935-4790

Electron Beam Microanalysis of Light Elements

CXRO is developing multilayers that can be used in electron probe microanalysers to do quantitative analysis of light elements such as fluorine, oxygen, nitrogen, carbon, and lithium. In the past this has been difficult due to a lack of crystals with a lattice period d large enough to diffract the long wavelength characteristic x-rays from these elements. Mica, for example, with a period (d) of 19.8 \AA , cannot be used for analysis of oxygen, whose $K\alpha$ emission is at 23.4 \AA , or nitrogen (33.2 \AA), or carbon (43.8 \AA). On the other hand, multilayer reflectors can be made with the required d -spacing and have been used as artificial crystals for microprobe analysis. Most have very low efficiency (1% or less). We have developed improved layered dispersion elements (LDEs) with efficiencies of 5% or more for these wavelengths. They allow the detection of the light elements with better signal to noise ratios and hence improved sensitivity. Figure 14 shows detection of the $K\alpha$ line of nitrogen (a) with a commercially available LDE with layer pairs of tungsten and silicon, and (b) with a new high reflectivity LDE developed at CXRO. The peak signal approximately 10 times greater for the CXRO device. Similar results have been obtained in the analysis of oxygen. This improvement in light element analysis capability has important applications in, for example, materials science and geochemistry, and may provide particularly important opportunities for industrial development.

Figure 14. The $K\alpha$ line of nitrogen (a) with a commercially available layered dispersion elements (LDEs) with layer pairs of tungsten and silicon, and (b) with a new high reflectivity LDE developed at CXRO. The peak signal is approximately 10 times greater for the CXRO-developed device.



XRL 937-4828

EUV / Soft X-ray Reflectometer

The ability to make accurate and reliable calibration measurements in the extreme ultraviolet/soft x-ray region is required to enable scientists and engineers to measure the performance of optical elements and predict the performance of a system. This need is driven by the current activity in projection lithography as well as a variety of studies using synchrotron radiation. Our present capability for making such measurements centers around our reflectometer using a laser-produced plasma EUV source, and shown in Figure 15. It uses a unique high throughput monochromator designed and built at CXRO that varies the wavelength to the optical elements being tested. Some recent studies, which include investigations of the stability of Mo/Si multilayer mirrors, and the development of multilayer coatings for imaging optics at short wavelength are described in the multilayer section of this annual report.

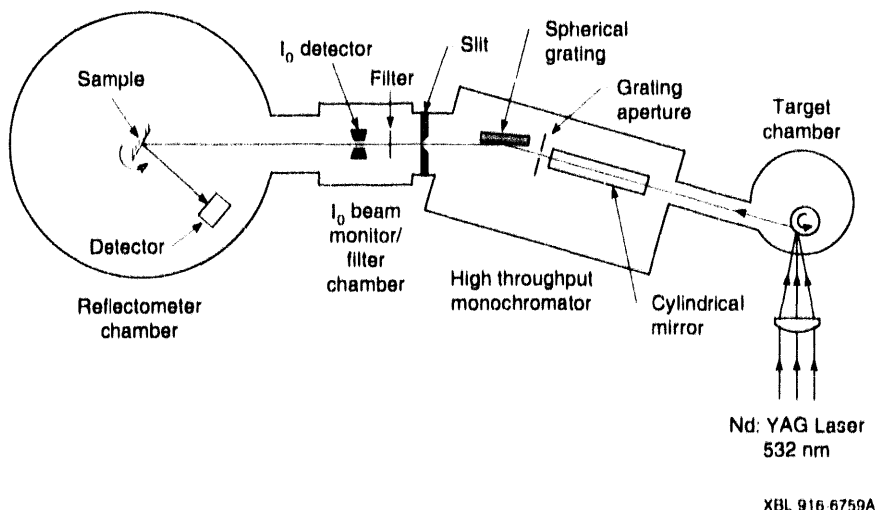


Figure 15. The CXRO extreme ultraviolet/soft x-ray reflectometer uses a laser-plasma source; the desired wavelength is selected from its broadband output with a unique high-throughput monochromator designed and built at LBL. (Conventional reflectometers use an x-ray tube of fixed wavelength.) The wavelength extends from about 30 to 100 Å.

There is also a continuing need for improved measurements of the optical constants of materials in order to be able to predict and understand the performance of optics. Particularly, in the soft x-ray/extreme ultraviolet spectral range the optical constants are poorly known because of the difficulties involved in their measurement. We have obtained the optical constants for a variety of materials using both transmission and reflection measurement. Our recent measurements of both the imaginary (absorptive) and real (dispersive) parts of the index of refraction of platinum are shown in Figure 16, in which the data shown were obtained from the angle dependence of the reflectivity of a smooth platinum mirror. The measurements are compared to the indices of refraction as calculated from our compilation of atomic scattering factors described in a later section of this annual report.

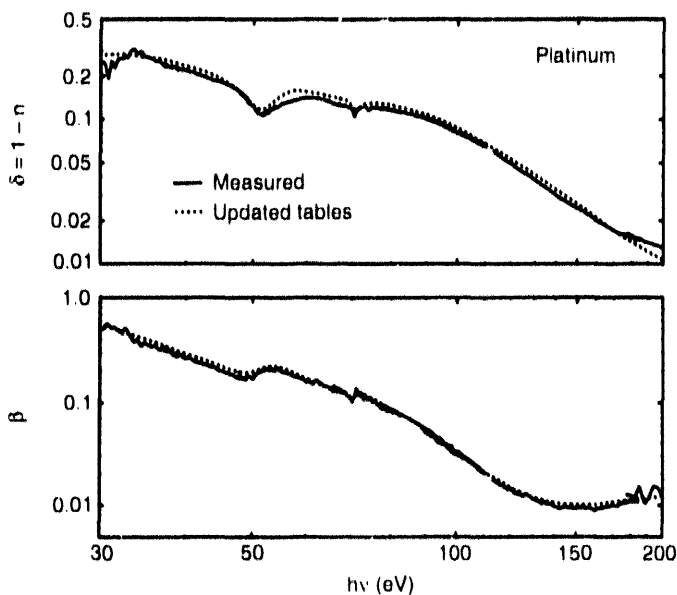


Figure 16. The measured indices of refraction of platinum (solid lines) and the indices of refraction as calculated from our recent tabulation of atomic scattering factors (dashed lines). The measurements were obtained by angular dependent reflectivity using the reflectometer described above.

XBL 937-4830

Photoemission Microscopy with Reflective Optics

Characterizations such as these will be performed with improved spectral and spatial resolutions and over a broader photon energy range at a bending magnet beamline under construction at the ALS. The emphasis of these beamlines will be absolute measurements with moderate spectral ($\lambda/\Delta\lambda \times 2000$) and spatial resolution ($\Delta x \approx 100 \mu\text{m}$).

A collaboration between the Center for X-Ray Optics and the Synchrotron Radiation Center at the University of Wisconsin has produced the first scanning soft x-ray microscope using reflective optics. Working at a wavelength of 130 \AA , the new microscope, shown in Figure 17, has demonstrated a spatial resolution of less than $0.1 \mu\text{m}$ and simultaneously an electron energy resolution of 350 millielectron volts (meV). This performance is significantly better than any achieved so far by alternative electron schemes. These developments are leading to a new generation of high spatial resolution surface analytical capabilities that will be important in understanding the heterogeneous nature of technologically and scientifically important surfaces on size scales ranging from several hundred angstroms upward. These features will become important as the Advanced Light Source begins operation.

The Center for X-Ray Optics designed and fabricated the critical reflective multilayer interference coatings that allow normal incidence focusing at very soft x-ray wavelengths. Molybdenum/silicon multilayers having individual film thicknesses of $30\text{-}40 \text{ \AA}$ were deposited onto the spherical surfaces of highly polished Schwarzschild objectives to provide reflectivities of 60% per surface at 130 \AA wavelength. Special techniques were developed to control the thickness of the multilayer coatings to ensure acceptable performance over the entire clear aperture of the optical system. The Center for X-Ray Optics also provided a custom designed monochromator and other beamline components to match the output of the undulator x-ray source to the microscope objective.

Figure 18 shows an example of the manner in which the microscope may be used to study surfaces with heterogeneous chemical structure. The

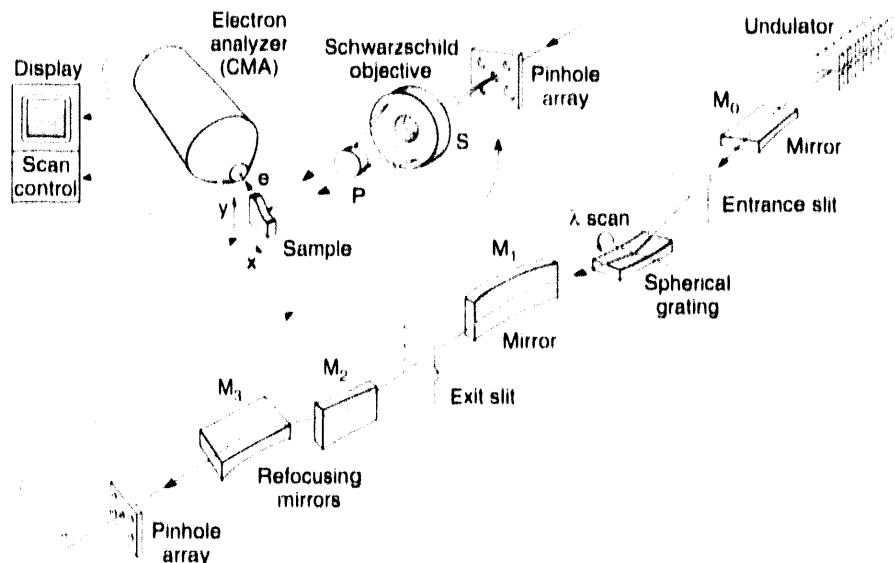


Figure 17. MAXIMUM Photoemission Microscope as installed at the University of Wisconsin's Synchrotron Radiation Center (SRC).

XBL 9211 5844

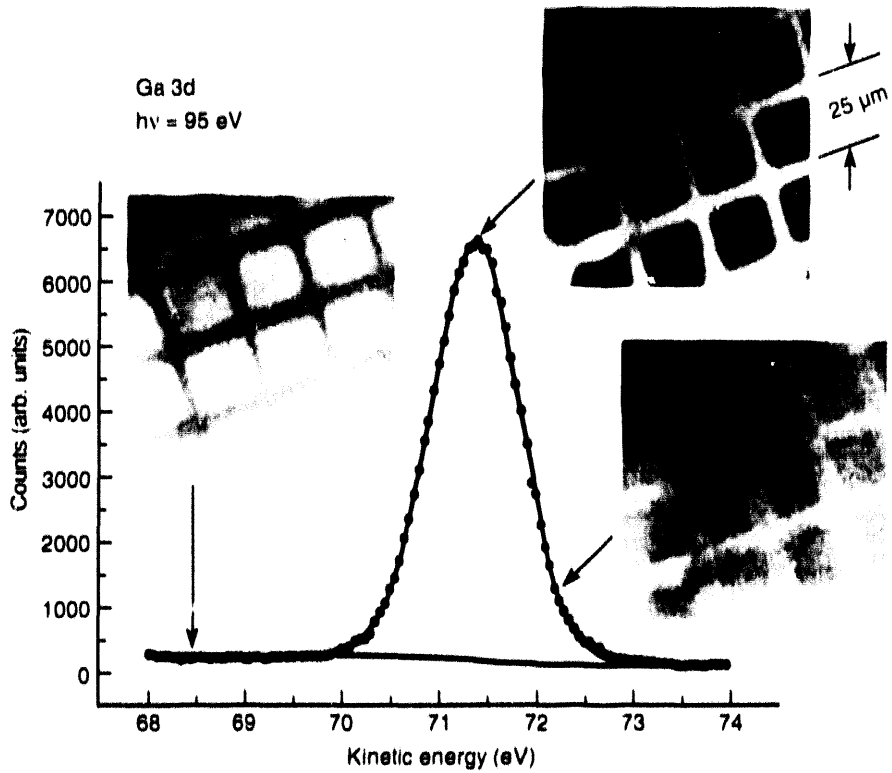


Figure 18. The energy distribution curve of the electrons emitted during a scan over the Ga 3d core level taken on a cleaved gallium arsenide surface. Left insert: secondary electrons from gold squares. Center insert: 3d electrons from gallium wire grid. Right insert: photoelectrons from both Ga and gold. MAXIMUM photoemission microscope, University of Wisconsin, Madison.

BBC 926-4899A

graph shows the energy distribution curve of the electrons emitted during a scan over the Ga 3d core level taken on a cleaved gallium arsenide surface. The surface of the GaAs was masked with a 25-μm mesh while 500 Å of gold was evaporated onto it, producing a pattern of gold squares. The inset images show spatial scans over 80 μm × 80 μm areas of the specimen, using a 0.5 μm spot, with the electron analyzer set at the three energies indicated by the arrows. The central image, set at the Ga 3d peak, is essentially a map of the gallium distribution. The left-hand scan shows the map of the secondary electrons from the gold and is essentially a gold image, while the right-hand image is composed of a combination of the two.

The Center for X-ray Optics has always been involved in the design, construction and implementation of new types of x-ray and extreme ultraviolet spectroscopic instrumentation, both for synchrotron radiation research and for other applications. We have continued our efforts to develop new spectroscopic instrumentation with desirable properties such as high resolution, high throughput, simplicity and low cost.

Spectroscopy with Soft X-Rays

Monochromators and Spectrometers

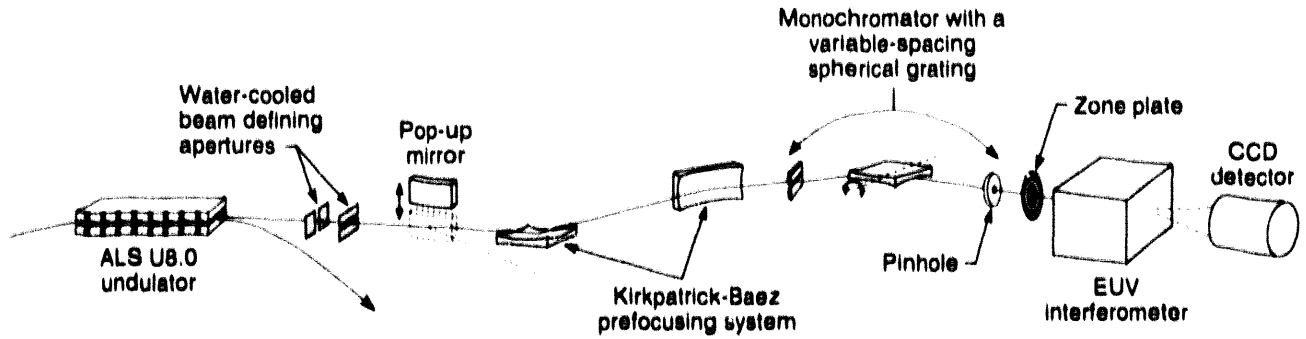
To achieve high spectral resolution without compromising throughput, we have continued our investigations into monochromators, spectrometers, and spectrographs using plane gratings with varied line spacing. Such gratings allow a flat (or erect) focal plane and can thus be scanned in wavelength without the complex scanning mechanisms required by more-conventional designs, such as spherical grating monochromators. One product of this work has been the High Resolution Streaked Spectrograph in use on the Nova laser at Lawrence Livermore National Laboratory. In addition, we have continued our studies of advanced monochromator and spectrometer designs for synchrotron radiation applications.

Recently we have developed computer codes that use ray-tracing techniques to simulate synchrotron radiation and estimate grating efficiency. In a theoretical study of such a monochromator in a U5.0 beamline at the ALS, we confirmed that it would provide high spectral resolution, high throughput, and small spot size. To put these results to the test of experiment, we are planning to build a new varied-line-spacing plane-grating monochromator for use at BESSY.

In another application-oriented program, we are investigating design options for dividing a soft x-ray beam among several users. This is challenging because an undulator source in a modern, low-emittance storage ring puts out a very thin, quasi-monochromatic beam that does not lend itself readily to either spatial or spectral splitting. The possibilities that we are examining include wavefront splitting, high-frequency timesharing, and splitting according to diffraction-grating order. The findings will be especially relevant for beamlines at third-generation synchrotron-light sources; the proposed ALS Life Sciences Center is a specific example.

Spatially and Temporally Coherent Beamlines

An undulator having a long periodic magnetic structure installed at a low emittance storage ring generates quasi-monochromatic, narrowly collimated, and partially coherent radiation. However, undulators currently operated and even those planned at third-generation synchrotron sources still do not provide a narrow bandwidth and a low enough emittance to meet spatial and temporal coherence requirements for experiments such as soft x-ray interferometry, holography, and scanning microscopy. We have explored beamline designs that comprise a variable-spacing spherical grating monochromator with a Kirkpatrick-Baez (KB) pre-focusing system to deliver a spatially and temporally coherent flux into an endstation without sacrificing throughput for the coherent flux radiated from the undulator. The designed system is schematically shown in Figure 19. The first mirror is a pop-up plane mirror for switching the incoming beam to the other station as well as for reducing heat load on the optics to follow. The KB prefocus system consists of the vertical-folding (KB₁) and horizontal-folding (KB₂) spherical mirrors, which focus the source image vertically on the entrance slit of the monochromator and horizontally on the exit slit (pinhole) respectively. The pinhole situated at the plane of the exit slit and the aperture in the endstation define the through-rays in the real and phase spaces, respectively. (By through rays we mean the rays that pass through both the pinhole and the aperture.) The product of effective sizes in the real and phase spaces compatible with the through rays are fairly close to those of the spatial coherence criterion.

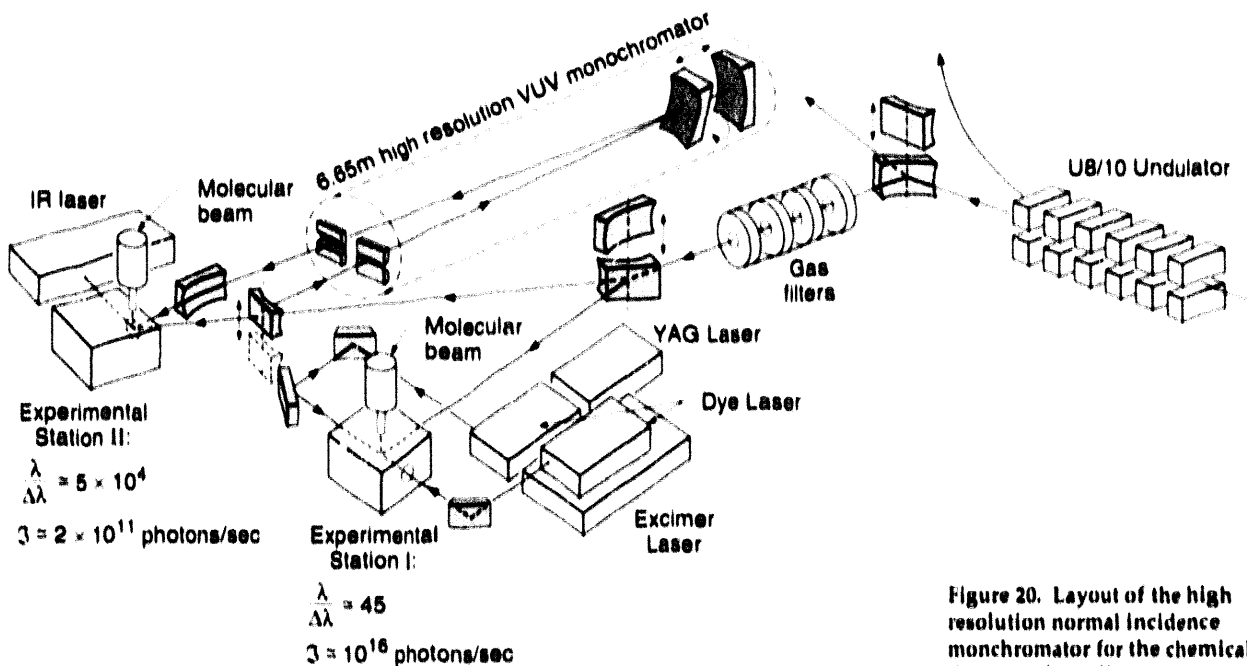


XBL 937-4825

Figure 19. Coherent radiation beamline consisting of a pop-up mirror, Kirkpatrick-Baez (KB) prefocusing mirrors, a variable spacing spherical grating monochromator, a pinhole-lens spatial filter, and an endstation. Beamlines such as this will be used for scanning x-ray microscopy, "at-wavelength" interferometry, and other applications requiring coherent EUV or soft-x-ray radiation.

Our design efforts have been extended to a high resolution VUV monochromator and its beamline to be devoted to chemical dynamics studies. The experimental system consists of a VUV high resolution monochromator beamline, infrared lasers, and molecular beam chambers (see Figure 20). The scientific research program will focus on gaining a rigorous molecular-level understanding of combustion and other energetic processes. An intense undulator radiation focused on a tenuous molecular beam enables one to observe transient molecules having very short life-

High Resolution VUV Monochromator for the Chemical Dynamics Beamline



XBL 937-4821

Figure 20. Layout of the high resolution normal incidence monochromator for the chemical dynamics beamline at the ALS.

times, and the higher spectral resolution is required to obtain more accurate information on energy levels involving such processes. To meet these needs, a 6.65-m off-plane Eagle monochromator, expected to attain a resolving power of over 50,000, will be installed in the beamline. However, a long focal length is only one of the factors required to obtain high resolution with high throughput. Other factors include use of a grating having high groove density and low aberrations. Therefore, design effort has been placed on compatibility between the various kinds of gratings and the monochromator. In the preliminary design we have investigated the performance of mechanically and holographically ruled gratings having variable spacing and curved grooves. The results show that the newly designed grating overcomes the shortcoming due to the astigmatism of a conventional grating and gives a minimum focal point size in the whole VUV scanning wavelength range without sacrificing the resolving power.

High Resolution Monochromator for Carbon-Related Studies

A high throughput, high resolution spectrograph based on a varied line-space grating has been installed on the two-beam x-ray laser chamber at the LLNL Nova laser facility. This instrument draws on our experience with a spectrograph that obtained a spectral resolving power $\lambda/\Delta\lambda$ of 35,000 in the measurement of the line width of an x-ray laser at wavelengths of 206 and 209 Å. It continues to be used for such high resolution spectrography projects as hyperfine structure, and has become invaluable for studying physical processes in x-ray lasers and other high temperature plasmas. This type of monochromator will have highest resolving power (about 17,000) around the K edge of carbon, i.e., about 45 Å, and thus will be useful for investigations related to the physics and chemistry of carbon and carbon-containing compounds. In addition to its high resolution capabilities the instrument will be able to make absolute x-ray wavelength measurements by using the grating spacing as a length standard. The prototype will be installed on a bending magnet beamline at the BESSY storage ring in Berlin, Germany, and a second will be installed at the Advanced Light Source.

Hard-X-Ray Microprobe

Elemental analysis by means of a high-energy x-ray microprobe using focused x-rays from a synchrotron source is characterized by high sensitivity, spatial resolution approaching 1 μm , ease of operation, and the ability to examine samples in a variety of environments. Elements are quantitatively and nondestructively detected by means of the characteristic fluorescent x-rays emitted by the irradiated sample. The photon energy identifies the element and the intensity measures its quantity. At present, elemental sensitivity of the microprobe reaches the femtogram level for elements from potassium to zinc in the periodic table. Additional detection sensitivity is imparted by the ability to select the x-ray photon energy to avoid excitation of interfering fluorescence from elements other than those being sought. A major advantage of the x-ray microprobe is that the specimen does not have to be kept in vacuum or subjected to special contrast-enhancing preparation. With tomographic techniques, it is possible to obtain depth distributions of elements within samples.



Figure 21. Installation of the x-ray microprobe beamline at the ALS is underway.



Applications of the microprobe occur in materials science (distribution of doping materials in semiconductors), geology (composition of inclusions in geological materials), environmental science (profiles of pollutants in animal tissue), biology (trace element analysis of biological materials), and archeology (analysis of ancient documents and artwork).

An x-ray microprobe beamline is being prepared for use in the earliest experiments at EBL's Advanced Light Source (ALS), a newly commissioned high brightness synchrotron facility. The new microprobe beamline will utilize multilayer coated optics and bending magnet radiation with photon energies extending from roughly 6 to 10 keV.

The research planned for this beamline emphasizes quantitative, spatially resolved trace element analysis of materials science samples. The trace element distribution within samples often determines structural properties. The x-ray microprobe will provide a sensitive nondestructive

X-Ray Microprobe Beamline at the ALS

tool for two-dimensional distribution of trace elements with a spatial resolution of 1 μm . The microprobe will be particularly useful for the characterization of defects and cracks in ceramic materials. Of particular interest are (1) cleavage or ductile fracture in bulk ceramic, such as partially stabilized zirconia, alumina, silicon carbide, and silicon nitride, or in ceramic composites, such as silicon carbide in alumina, (2) subcritical crack growth by stress corrosion or fatigue, and (3) fracture at the ceramic metal interface in metal-matrix composites, such as SiC-Al₂O₃. It is particularly important to determine whether crack processes occur in the bulk or only at the surface. The movement of different elements during annealing, mechanical stress, and chemical processing will also be studied.

The Advanced Light Source (ALS) is a national facility for scientific research and development, where work may be conducted as a member of a participating research team (PRT). The microprobe PRT consists of members of the Materials Sciences, Applied Sciences, Earth Sciences, and Engineering Sciences divisions of LBL as well as members from the Oak Ridge National Laboratory and the Lawrence Livermore National Laboratory. Beamline 10.3 will have two white-radiation branches. One experimental station will be dedicated to materials science experiments; the other will be used to develop advanced x-ray optical components and instrumentation.

Coronary Angiography

X-ray beams from a synchrotron source—monochromatic, well-collimated, and intense—provide unique opportunities for medical imaging. One of them is a new method of coronary angiography that uses venous injection of contrast agent, as opposed to arterial injection. For several years we have participated in a collaboration that is working on this new, safer method. A new step toward large-scale tests of clinical applicability was taken in 1990 with the completion of a dedicated medical-imaging facility on a special wiggler beamline at the NSLS. Eleven patients' hearts have been imaged there; the results are not yet equivalent to conventional angiograms, but they are approaching clinical usefulness, and the technique is dramatically easier and safer for the patients.

This year the imaging system at the NSLS was upgraded in two ways: A new Laue monochromator was installed, which increased the available x-ray flux by a factor of 8 over the previous monochromator. A new LBL-built detector with 1200 elements was also installed that replaced the previous 600-element detector. The computer system and data-acquisition software were also upgraded. The new system was tested in September 1993, and will be used with patients in early 1994.

Images obtained with the old system thus far clearly indicate that large portions of both the left anterior and the right coronary arteries can be examined with this method. Various changes are now underway to further improve the image quality. Then a medical research team will begin to use this technique on a large group of patients, comparing the new method to standard coronary angiography and also studying the effect of various medical treatments on the progression of coronary artery disease. An example of the image thus far achieved is shown by Figure 22.

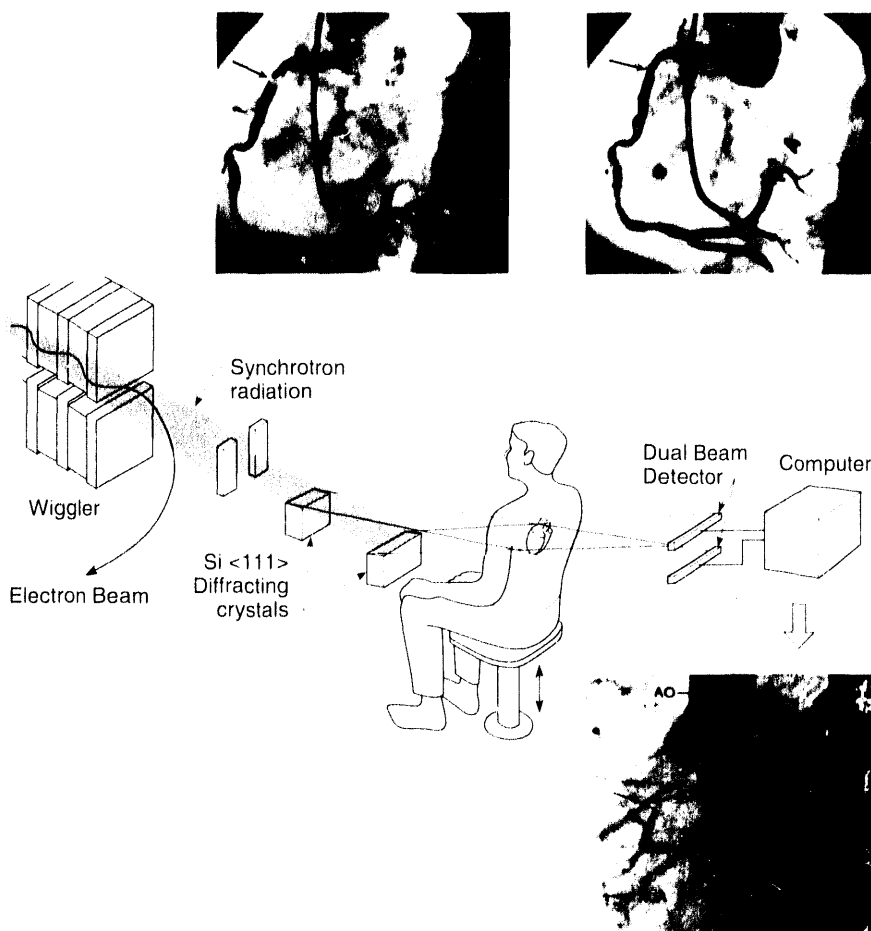


Figure 22. Angiograms made with a standard arterial injection of contrast agent, an invasive and relatively dangerous procedure, are shown at top left and right. At the lower right is an angiogram of the same patient taken with the synchrotron-radiation method, which uses a much less hazardous venous injection. The left image was taken just before a balloon angioplasty operation to clear a blockage (see arrow in image) in the right coronary artery (RCA). The top right image was taken just after the operation and the lower right image was taken 6 months later. The image quality of the lower right image, while not yet as good as the upper two images, shows clearly that coronary arteries can be clearly seen with the less invasive venous injection method. The significantly reduced hazard may permit studies of the progression of heart disease, and might some day be useful for clinical studies.

XBB 937-5003A

An extended tabulation of the atomic scattering factors, which describe the basic interaction of x-rays with matter, has been completed this past year, and is scheduled to be published in a special issue of the *Atomic Data and Nuclear Data Tables* in July 1993. These tables represent a revision of the 1982 compilation by Henke et al., which are widely used throughout the x-ray community. The revision is based on experimental measurements that have been published during the past 10 years as well as improved theoretical calculations. The range is extended to cover photon energies from 50 to 30,000 eV for the elements $Z = 1$ to 92. They are also being freely distributed on computer disk.

In order to improve our knowledge of the atomic scattering factors, better measurements will be required. Such data are currently obtained from measurements of the transmission through a thin film or the reflection from a smooth surface, or by x-ray interferometry. Measurements have been performed using our present sources (see the XUV Reflectometer section) and will be extended with the use of beamlines now under construction at the ALS.

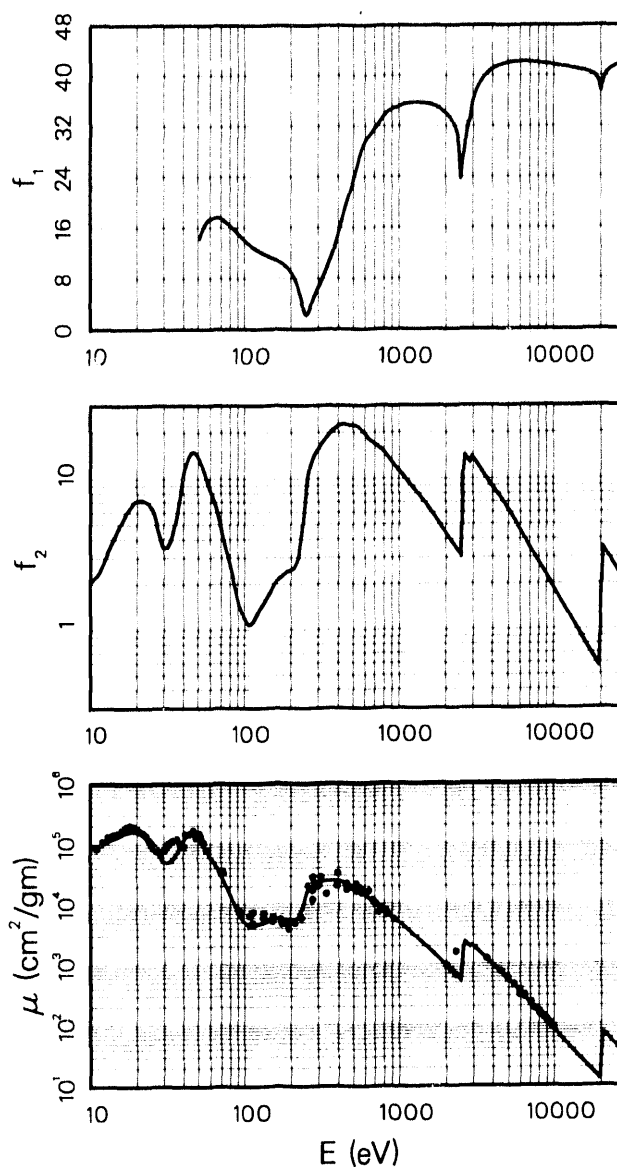
Atomic Scattering Factors

$$\mu_a(\text{barns/atom}) = \mu(\text{cm}^2/\text{gm}) \times 159.31$$

$$E(\text{keV})\mu(\text{cm}^2/\text{gm}) = f_2 \times 438.59$$

Molybdenum (Mo)
Z = 42
Atomic Weight = 95.940

Line	E(eV)	$\mu(\text{cm}^2/\text{gm})$	f_1	f_2	$\lambda(\text{\AA})$
H	10.2	9.03e+4		2.10	1215
He I	21.2	1.50e+5		7.27	584.3
Na L _{2,3}	30.5	5.08e+4		3.53	407.2
Mg L _{2,3}	49.3	1.26e+5		14.17	251.5
Al L _{2,3}	72.4	2.47e+4	17.21	4.08	171.2
Si L _{2,3}	91.5	7.03e+3	14.96	1.47	135.5
Be K	108.5	4.36e+3	13.32	1.08	114.3
Sr M ζ	114.0	4.37e+3	12.88	1.14	108.8
Y M ζ	132.8	4.94e+3	11.87	1.50	93.4
Zr M ζ	151.1	5.57e+3	11.12	1.92	82.1
B K α	183.3	5.71e+3	9.94	2.39	67.6
Mo M ζ	192.6	5.60e+3	9.45	2.46	64.4
Ar L ℓ	220.1	5.70e+3	6.86	2.86	56.3
C K α	277.0	2.14e+4	4.54	13.50	44.8
Ag M ζ	311.7	2.37e+4	7.56	16.85	39.8
N K α	392.4	2.45e+4	14.36	21.89	31.6
Ti L α	452.2	2.19e+4	20.06	22.61	27.4
V L α	511.3	1.91e+4	24.12	22.32	24.2
O K α	524.9	1.85e+4	25.11	22.13	23.6
Cr L α	572.8	1.59e+4	28.23	20.70	21.6
Mn L α	637.4	1.26e+4	30.36	18.34	19.5
F K α	676.8	1.13e+4	31.17	17.41	18.3
Fe L α	705.0	1.05e+4	31.74	16.83	17.6
Co L α	776.2	8.77e+3	33.11	15.53	16.0
Ni L α	851.5	7.12e+3	34.34	13.82	14.6
Cu L α	929.7	5.80e+3	34.90	12.30	13.3
Zn L α	1011.7	4.84e+3	35.19	11.17	12.3
Na K α	1041.0	4.54e+3	35.34	10.78	11.9
Ge L α	1188.0	3.35e+3	35.68	9.07	10.4
Mg K α	1253.6	2.96e+3	35.73	8.46	9.9
Al K α	1486.7	1.98e+3	35.61	6.71	8.3
Si K α	1740.0	1.35e+3	35.07	5.36	7.1
Zr L α	2042.4	9.11e+2	33.83	4.24	6.1
Mo L α	2293.2	6.84e+2	31.73	3.57	5.4
Cl K α	2622.4	2.20e+3	27.66	13.13	4.7
Ag L α	2984.3	2.02e+3	35.52	13.78	4.2
Ca K α	3691.7	1.20e+3	40.27	10.06	3.4
Ti K α	4510.8	7.12e+2	41.71	7.32	2.7
V K α	4952.2	5.57e+2	41.99	6.28	2.5
Cr K α	5414.7	4.39e+2	42.14	5.42	2.3
Mn K α	5898.8	3.49e+2	42.19	4.69	2.1
Co K α	6930.3	2.25e+2	42.13	3.56	1.8
Ni K α	7478.2	1.83e+2	42.07	3.12	1.7
Cu K α	8047.8	1.50e+2	41.99	2.75	1.5
Ge K α	9886.4	8.50e+1	41.72	1.92	1.3
Y K α	14988.0	2.67e+1	40.91	0.91	0.8
Mo K α	17479.0	1.74e+1	40.36	0.70	0.7
Pd K α	21177.0	6.97e+1	39.98	3.37	0.6
Sn K α	25271.0	4.37e+1	41.59	2.52	0.5
Xe K α	29779.0	2.80e+1	42.02	1.90	0.4



Edge Energies

K	19999.5 eV	L _I	2865.5 eV	M _I	506.3 eV ^b	N _I	63.2 eV ^b
		L _{II}	2825.1 eV	M _{II}	411.6 eV ^b	N _{II}	37.6 eV ^b
		L _{III}	2520.2 eV	M _{III}	394.0 eV ^b	N _{III}	35.5 eV ^b
				M _{IV}	231.1 eV ^b		
				M _V	227.9 eV ^b		

References: 33, 48, 52, 59, 76, 115, 123, 127, 131, 177, 200, 205, 223, 233.

Figure 23. The atomic scattering factors for molybdenum as will appear in the special issue of *Atomic Data and Nuclear Data Tables* in July 1993. This tabulation covers the extended range of 50 to 30,000 eV for all elements from hydrogen (Z = 1) to uranium (Z = 92).

Ade, H., C.H. Ko and E. Anderson, "Astigmatism Correction in X-Ray-Scanning Photoemission Microscope with Use of Elliptical Zone Plate," *App. Phys. Lett.*, **60**, 1040 (1992).

Ade, H., C.H. Ko, E.D. Johnson and E. Anderson, "Improved Images with the Scanning Photoelectron Microscope at the National Synchrotron Light Source," *Surface and Interface Analysis*, **19**, 17 (1992).

Anderson, E.H., V. Boegli, M.L. Schattenburg, D. Kern and H.I. Smith, "Metrology of Electron-Beam Lithography Systems Using Holographically Produced Reference Sample," *J. of Vac. Sci. & Tech. B*, **9**, 3606 (1991).

Anderson, E., D. Kern, "Nanofabrication of Zone Plates for X-ray Microscopy," in *X-ray Microscopy III*, A.G. Michette, G.R. Morrison, C.J. Buckley, Eds., Springer Series in Optical Sciences **67** (Springer-Verlag, New York, 1992), 75-78.

Attwood, D.T., "New Opportunities at X-ray Wavelengths," *Physics Today*, Am. Inst. Physics, NY (August 1992).

Attwood, D., G. Sommargren, R. Beguiristain, K. Nguyen, J. Bokor, N. Ceglie, K. Jackson, M. Koike, and J. Underwood, "Undulator Radiation for Extreme Ultraviolet Interferometry of Projection Lithography Optics," *Appl. Opt.* (to be published).

Balhorn, R., M. Corzett, M. Allen, C. Lee, T. Barbee, Jr., J. Koch, B. MacGowan, D. Matthews, S. Mrowka, J. Trebes, I. McNulty, L. Da Silva, J. Gray, E. Anderson, D. Kern, D. Attwood, "Application of X-rays to the Analysis of DNA Packaging in Mammalian Sperm," in *Soft X-ray Microscopy*, C. Jacobsen, J. Trebes, Eds., Proc. SPIE 1741, 43 (1992)

DaSilva, L.B., J.E. Trebes, R. Balhorn, S. Mrowka, E. Anderson, D.T. Attwood, T.W. Barbee, Jr., J. Brase, M. Corzett, J. Gray, J.A. Koch, C. Lee, D. Kern, R.A. London, B.J. MacGowan, D.L. Matthews and G. Stone, "X-ray Laser Microscopy of Rat Sperm Nuclei," *Science* **258**, 269 (1992).

De Stasio, G., C. Capasso, W. Ng, A.K. Ray-Chaudhuri, S.H. Liang, R.K. Cole, Z.Y. Guo, J. Wallace, F. Cerrina, G. Margaritondo, J. Underwood, R. Perera, J. Kortright, D. Mercanti, M.T. Ciotti, and A. Stecchi, "High Resolution Photoelectron Microimaging of Neuron Networks," *Europhysics Letters*, **16**, 411 (1991).

Dilmanian, F.A., E. Nachaliel, R.F. Garrett, W.C. Thomlinson, L.D. Chapman, H.R. Moulin, T. Oversluisen, H.R. Rarback, M. Rivers, P. Spanne, A.C. Thompson and H.D. Zeman, "Multiple Energy Computed Tomography with Monochromatic X-rays from the NSLS," *IEEE Conf. Record of the Medical Imaging Conference*, **3**, 1831 (1992).

Goncz, K., M. Moronne, W. Lin, S. Rothman, "Measuring Changes in the Mass of Single Subcellular Organelles using X-ray Microscopy," in *Soft X-ray Microscopy*, C. Jacobsen, J. Trebes, Eds., Proc. SPIE 1741, 40 (1992).

Gullikson, E.M., J.H. Underwood, P.C. Batson, and V. Nikitin, "A Soft X-ray/EUV Reflectometer Based on a Laser-Produced Plasma Source," *J. of X-ray Sci. and Tech.*, **3**, 258 (1992).

Henke, B.L., E.M. Gullikson and J.C. Davis, "X-Ray Interactions: Photoabsorption, Scattering, and Reflection. E = 50-30,000 eV, Z = 1-92," *Atomic Data and Nuclear Data Tables*, **54**, No. 2 (Academic Press, San Diego (1993).

Kagoshima, Y., J. Wang, M. Ando, S. Aoki, E. Anderson, D. Attwood, and D. Kern, "70 nm-Resolution Zone Plate Soft X-ray Microscope using Undulator Radiation," *Japn. J. Appl. Physics* (in press).

Koch, J.A., B.J. MacGowan, L.B. DaSilva, D.L. Matthews, J.H. Underwood, P.J. Batson, and S. Mrowka, "Observation of Gain-Narrowing and Saturation in Se X-ray Laser Line Profiles," *Phys. Rev. Lett.* **68**, 3291 (1992).

Koike, "Beam Splitting of Undulator Radiation with Variable Spacing Plane Grating Monochromator," *Nucl. Instru. Methods*. **A319**, 135-140 (1992).

Kortright, J.B., E.M. Gullikson, and P.E. Denham, "Masked Deposition Techniques for Achieving Multilayer Period Variations Required for Short Wavelength (68Å) Soft X-ray Imaging Optics," *Applied Optics* (accepted).

Kortright, J.B., H. Kimura, V. Nikitin, K. Mayama, M. Yamamoto, and M. Yanagihara, "Soft X-ray (97 eV) Phase Retardation Using Transmission Multilayers," *Applied Physics Letters*, **60**, 2963 (1992).

Matthews, D. L., D. Minyard, G. Stone, T. Yorkey, E.H. Anderson and D.T. Attwood, "Demonstration of X-Ray Microscopy with an X-Ray Laser Operating near the Carbon K Edge," *Optics Letters*, **17**, 754 (1992).

- McNulty, L., J. Kirz, C. Jacobsen, E.H. Anderson, M.R. Howells, and D.P. Kern, "High-Resolution Imaging by Fourier-Transform X-Ray Holography," *Science*, **256**, 1009 (1992).
- Meyer-Ilse, W., P. Guttman, J. Thieme, D. Rudolph, G. Schmah, E. Anderson, P. Batson, D. Attwood, N. Iskander, D. Kern, "Experimental Characterization of Zone Plates for High Resolution X-ray Microscopy," in *X-ray Microscopy III*, A.C. Michette, G.R. Morrison, C.J. Buckley, Eds., Springer Series in Optical Sciences **67** (Springer-Verlag, New York, 1992), 284-289.
- Meyer-Ilse, W., M. Koike, H. Beguiristain, J. Maser, D. Attwood, "X-ray Microscopy Resource Center at the Advanced Light Source", in *Soft X-ray Microscopy*, C. Jacobsen, J. Trebes, Eds., Proc. SPIE 1741, 9 (1992).
- Meyer-Ilse, W., D. Attwood, and M. Koike, "X-ray Microscopy Resource Center at the Advanced Light Source," in Proceedings of the BSR '92 Conference on Biology and Synchrotron Radiation: *Synchrotron Radiation in the Life Sciences* (Oxford University Press, New York, 1993).
- T. Namioka and M. Koike, "Analytical Representation of Spot Diagrams and its Application to the Design of Monochrometers," *Nucl. Inst. and Meth.* **A319**, 219-227 (1992)
- T. Namioka and M. Koike, "Design of Compact High-Resolution Far-Ultraviolet Spectrographs Equipped with a Grating Having Variable Spacing Curved Grooves," *UV and X-Ray Spectroscopy of Astrophysical and Laboratory Plasmas*, AIP Conference Proceedings (in press).
- Nachaliel, E., F.A. Dilmanian, R.F. Garrett, W.C. Thomlinson, N.G. Gmur, N.M. Lazarz., H.R. Moulin, M.L. Rivers, H. Rarback, P.M. Stefan, P. Spanne, P.N. Luke, R. Pehl, A.C. Thompson and M. Miller, "Monochromatic Computed Tomography of the Human Brain using Synchrotron X-Rays: Technical Feasibility," *Nucl. Inst. and Meth.* **A319**, 305 (1992).
- Nguyen, K.B., T. D. Nguyen, D.T. Attwood, F.K. Gustafson, "Step Coverage Profile and Propagation of Roughness of Sputter-Deposited Multilayer Coating for EUV Projection Lithography," *J. Vac. Sci. Technol.* (to be published).
- Nguyen, K.B., T. D. Nguyen, A.K. Wong, A.R. Neureuther, D.T. Attwood, "Areal Images of EUV Projection Lithography Masks with Defects in Reflective Coatings: Electromagnetic Stimulation," *OSA Proceedings for Soft X-ray Projection Lithography '93* (to be published).
- Nguyen, T.D., R. Gronsky, and J.B. Kortright, "Microstructural Evolution of Nanometer Ruthenium Films Between Carbon Layers with Thermal Treatments," *Mat. Res. Soc. Proc.*, **230**, 109 (1992).
- Smith, H.I., S.D. Hector, M.L. Schattenburg, and E.H. Anderson, "A New Approach to High Fidelity E-Beam and Ion-Beam Lithography Based on an In Situ Global Fiducial Grid," *J. of Vac. Sci. & Tech. B*, **6**, 2992 (1992).
- Thomlinson, W., N. Gmur, D. Chapman, R. Garrett, N. Lazarz, H. Moulin, A.C. Thompson, H.D. Zeman, G.S. Brown, J. Morrison, P. Reiser, V. Padmanabahn, L. Ong, S. Green, J. Giacomini, H. Gordon and E. Rubenstein, "First Operation of the Medical Research Facility at the NSLS for Coronary Angiography," *Rev. Sci. Instr.* **63**, 625 (1992).
- Thompson, A.C., K.L. Chapman *et al.*, "Focussing Optics for a Synchrotron-Based X-Ray Microprobe," *Nucl. Inst. and Meth.* **A319**, 305 (1992).
- Thompson, A.C., K.L. Chapman, and J.H. Underwood, "Development of an X-ray Microprobe Using Synchrotron Radiation," *SPIE Proc. of Conf. on Optics for High-Brightness Synchrotron Beamlines*, July, 1992 (**in press**).
- Underwood, J.H., E.M. Gullikson, and K. Nguyen, "Tarnishing of Mo/Si Multilayer X-ray Mirrors," *Applied Optics* (to be published).
- Underwood, J.H., J.B. Kortright, R.C.C. Perera, F. Cerrina, C. Capasso, A.K. Ray-Chaudhuri, W. Ng, J. Welna, J. Wallace, S. Liang, and G. Margaritondo, "X-ray Microscopy with Multilayer Mirrors: the MAXIMUM Photoelectron Microscope," Proceedings of the BSR '92 Conference: *Synchrotron Radiation in the Life Sciences* (Oxford University Press, New York, 1993).
- Yen, A., E.H. Anderson, R.A. Ghanbari, M.L. Schattenburg, and H.I. Smith, "Achromatic Holographic Configuration for 1100-nm-Period Lithography," *Applied Optics*, **31**, 4540 (1992)

